Emergent Cell-free layer Asymmetry and Biased Haematocrit Partition in a Biomimetic Vascular Network of Successive Bifurcations

Electronic Supplementary Information (ESI)

Qi Zhou[1,*], *Joana Fidalgo*[2], *Miguel O. Bernabeu*[3], *Mónica S. N. Oliveira*[2], *Timm Krüger*[1,*]

1. School of Engineering, Institute for Multiscale Thermofluids, University of Edinburgh, Edinburgh EH9 3FB, UK
2. James Weir Fluids Laboratory, Department of Mechanical and Aerospace Engineering, University of Strathclyde, Glasgow G1 1XJ, UK
3. Centre for Medical Informatics, Usher Institute, University of Edinburgh, Edinburgh EH16 4UX, UK
** Corresponding authors: q.zhou@ed.ac.uk; timm.krueger@ed.ac.uk*

S1 Validation of biomimetic network design

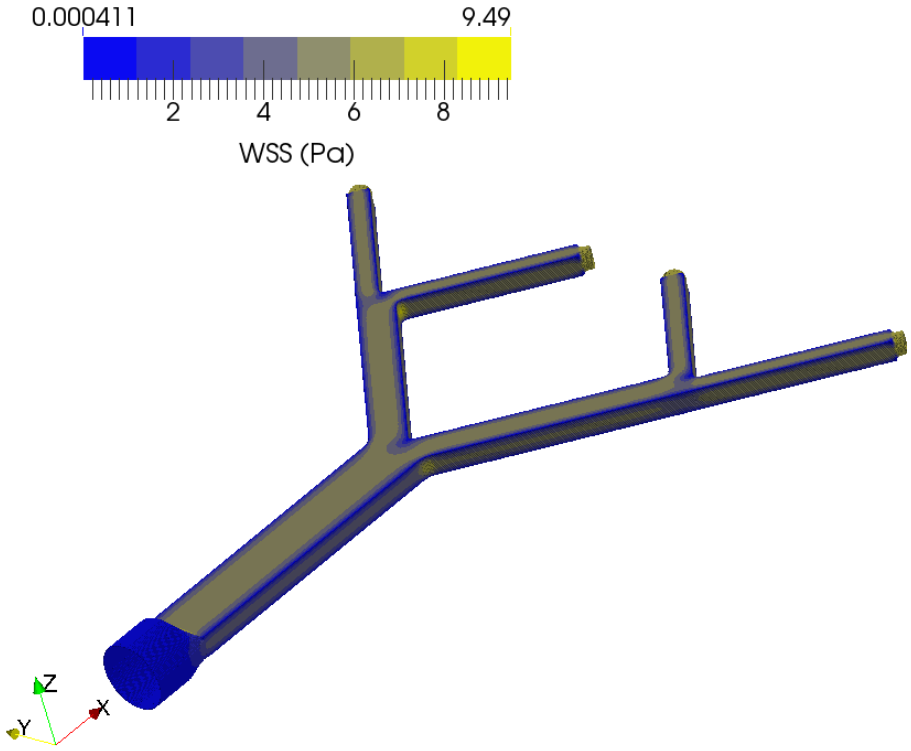

Figure S1: (Simulation) Unperturbed flow under $Q_2/Q_1 = 1$, with the contour demonstrating constant wall shear stress in the fully developed regions throughout the network.

S2 Network design with 60-degree bifurcations

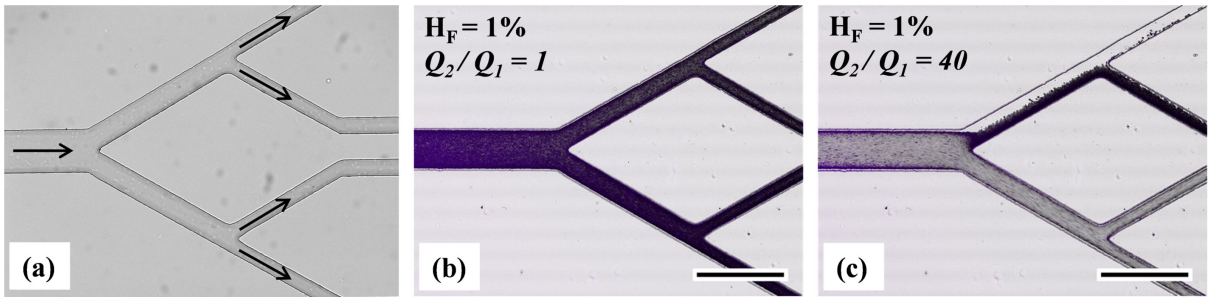

Figure S2: (Experiment) (a) A second design of the network with identical W_i and H but different bifurcation angles, which are all 60 degrees in this geometry. Composite images obtained using the Z-projection method (minimum intensity), each combining multiple video frames of the same region to show the RBC distribution under different outflow ratios Q_2/Q_1: (b) 1 and (c) 40. For both (b,c), $H_F = 1\%$. Note that all experimental images in this figure have been rotated by 90 degrees for visual clarity.

S3 Visualisation of RBCs and flow pathlines

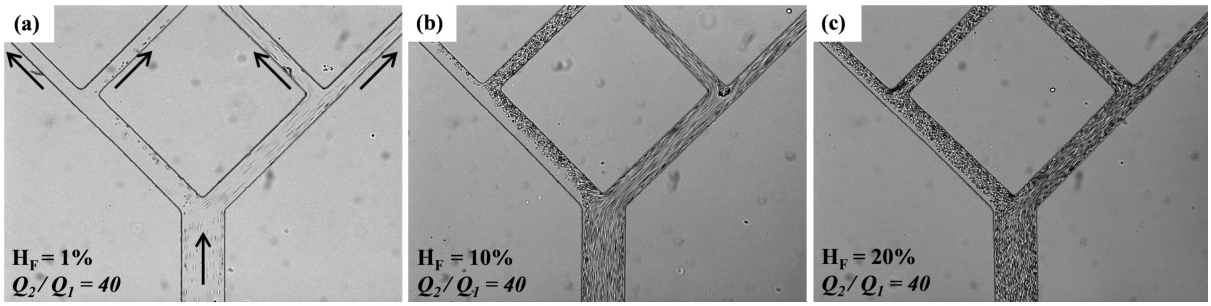

Figure S3: (Experiment) Individual experiment frames showing RBCs flowing through the bifurcating network under a fixed outflow ratio of $Q_2/Q_1 = 40$ ($Q_1 = 0.2$ μL/min and $Q_2 = 8.0$ μL/min), for (a) $H_F = 1\%$, (b) $H_F = 10\%$ and (c) $H_F = 20\%$.

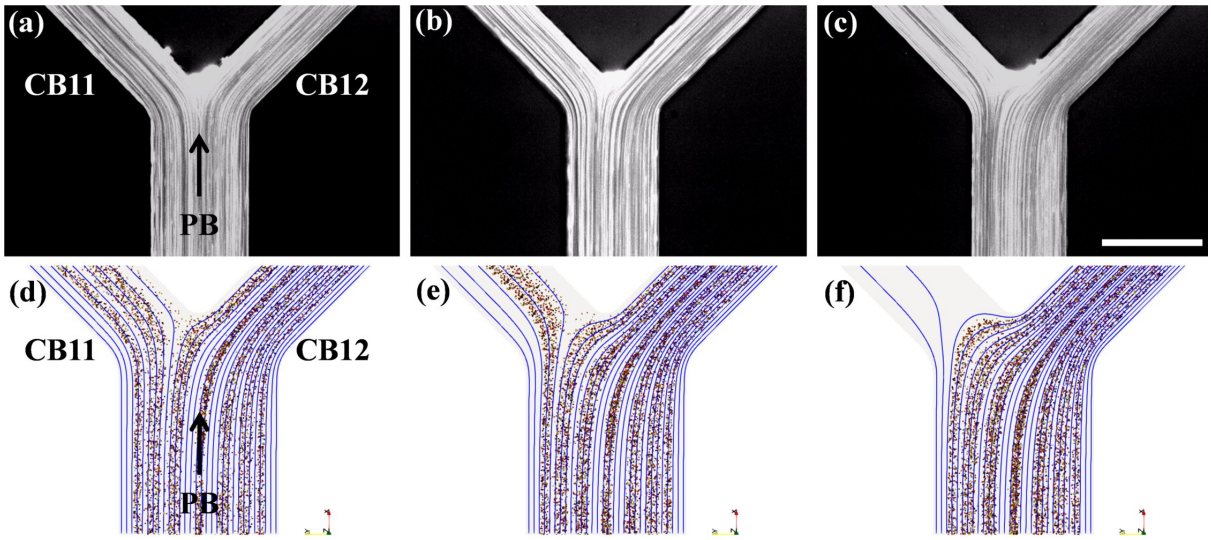

Figure S4: (a–c) (Experiment) Flow pathlines of fluorescent particles in a $H_F = 1\%$ suspension flowing under different outflow ratios: (a) $Q_2/Q_1 = 1$; (b) $Q_2/Q_1 = 6$; (c) $Q_2/Q_1 = 40$. (d–f) (Simulation) Comparison of RBC trajectories with streamlines at $Q_2/Q_1 = 3$, 9, and 39, respectively. For each flow condition, 100 RBCs are randomly selected. The coloured dots represent centres of mass of RBCs throughout the simulation. Note that both experimental and simulation images in this figure have been rotated by 90 degrees for visual clarity.

S4 Deformation of RBCs under varying shear

Table S1: (Simulation) Characteristic capillary number Ca throughout the simulated branching network under different flow conditions ($Q_2/Q_1 = 3$, 9, 19, 39). Ca is evaluated at the wall of an equivalent circular channel with the same hydraulic diameter.

Q_2/Q_1	PB	CB11	CB12	CB21	CB22	CB23	CB24
3	0.6	0.35	1.04	0.37	0.37	1.10	1.10
9	0.6	0.14	1.25	0.15	0.15	1.32	1.32
19	1.0	0.12	2.19	0.12	0.12	2.32	2.32
39	0.6	0.03	1.35	0.04	0.04	1.43	1.43

As the simulated RBCs travel through the network, distinct shapes are observed (Figure S5). In response to the local fluid shear, their morphology can substantially deviate from the unstressed biconcave shape (Fig. S5a), and evolves into a either stretched or folded structure (Figure S5b–i). For $Q_2/Q_1 \neq 1$, the bifurcating network creates an environment of varying shear and different values of the capillary number Ca exist (see Table S1), where Ca characterises the cell deformation and is defined as in Equation 2 of the main text. As the magnitude of shear experienced by the RBCs increases (reflected by the local Ca estimated at an RBC's centre of mass), three-dimensional features, such as membrane lobes, develop. These membrane deformations are reversible and can be flattened as the RBC relaxes after entering a region with reduced shear.

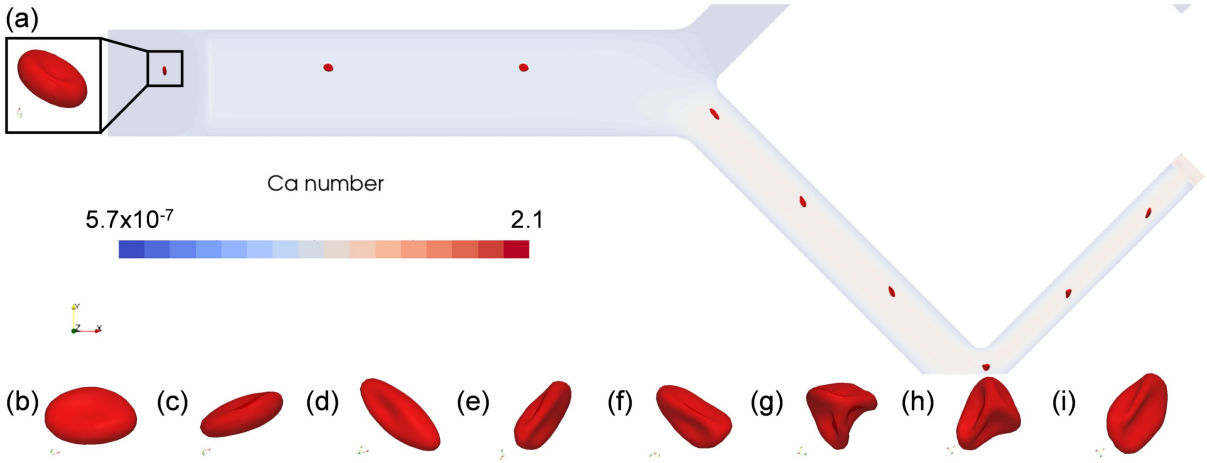

Figure S5: Shape variation of an RBC subject to varying shear along its path. (a) A snapshot of the unperturbed flow simulation $Q_2/Q_1 = 19$ overlaid with time sequence of an RBC (viscosity contrast $\lambda = 1$) extracted from a $H_F = 1\%$ suspension simulated under identical flow conditions, travelling downwards PB, CB12 and CB23. The inset shows an enlarged (and rotated for visual clarity) view of the initial RBC shape (a biconcave discoid). The contour indicates the pattern of capillary number Ca in the bifurcating network. (b–i) show the RBC at the other eight locations. The local value of Ca estimated at the centre of mass of the RBC are (b) $Ca = 0.01$, (c) $Ca = 0.02$, (d) $Ca = 0.17$, (e) $Ca = 0.17$, (f) $Ca = 0.15$, (g) $Ca = 0.56$, (h) $Ca = 0.15$, (i) $Ca = 0.14$, respectively.

S5 Development of cell-free layer

To validate the numerical treatment of the flow inlet in the present study, the spatial development of the simulated CFLs in the parent branch of the present study is compared against the scaling law derived earlier in our previous work [1] for a straight channel of identical cross-section (Figure S7). The same scaling of CFL growth against development length is found in the depthwise direction (including CFLs at the top/bottom walls) under all investigated flow ratios, showing power-law increase with an exponent of 1/3 (Figure S7a–d). Contrarily, the widthwise CFLs (*i.e.* those at the left/right walls) show negligible increase in thickness, indicated by a small growth rate of nearly zero. The heavily slowed CFL growth in the parent branch of the present network compared to the previous straight channel can be explained by the magnitude of the initial CFL resulting from the numerical treatment, *i.e.* 6–7 μm, which is large enough to substantially alter the scaling law of CFL development according to our previous finding [1].

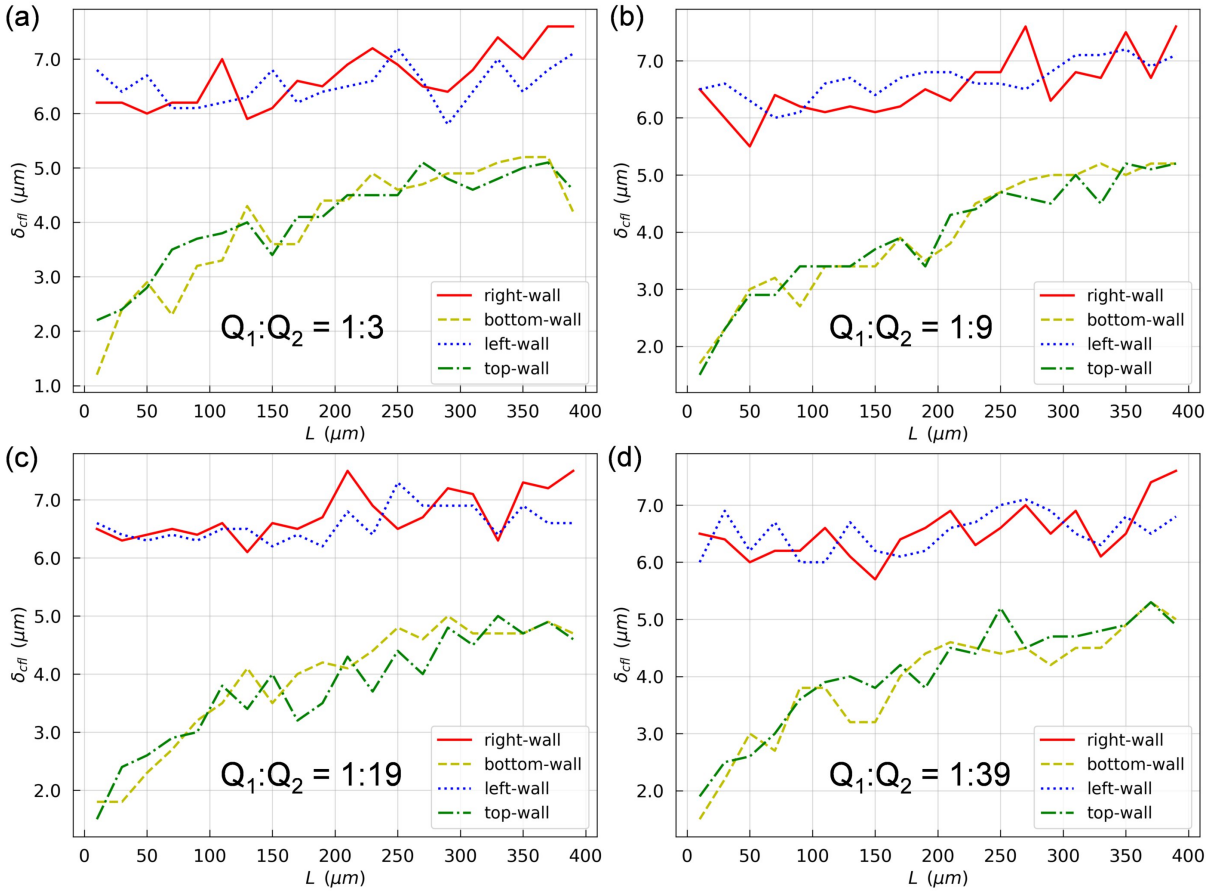

Figure S6: (Simulation) CFLs along the channel axis of PB (at right/bottom/left/top walls) plotted as the CFL thickness δ_{cfl} against the development length L. L is measured from the entrance of the PB till arriving at the bifurcation region.

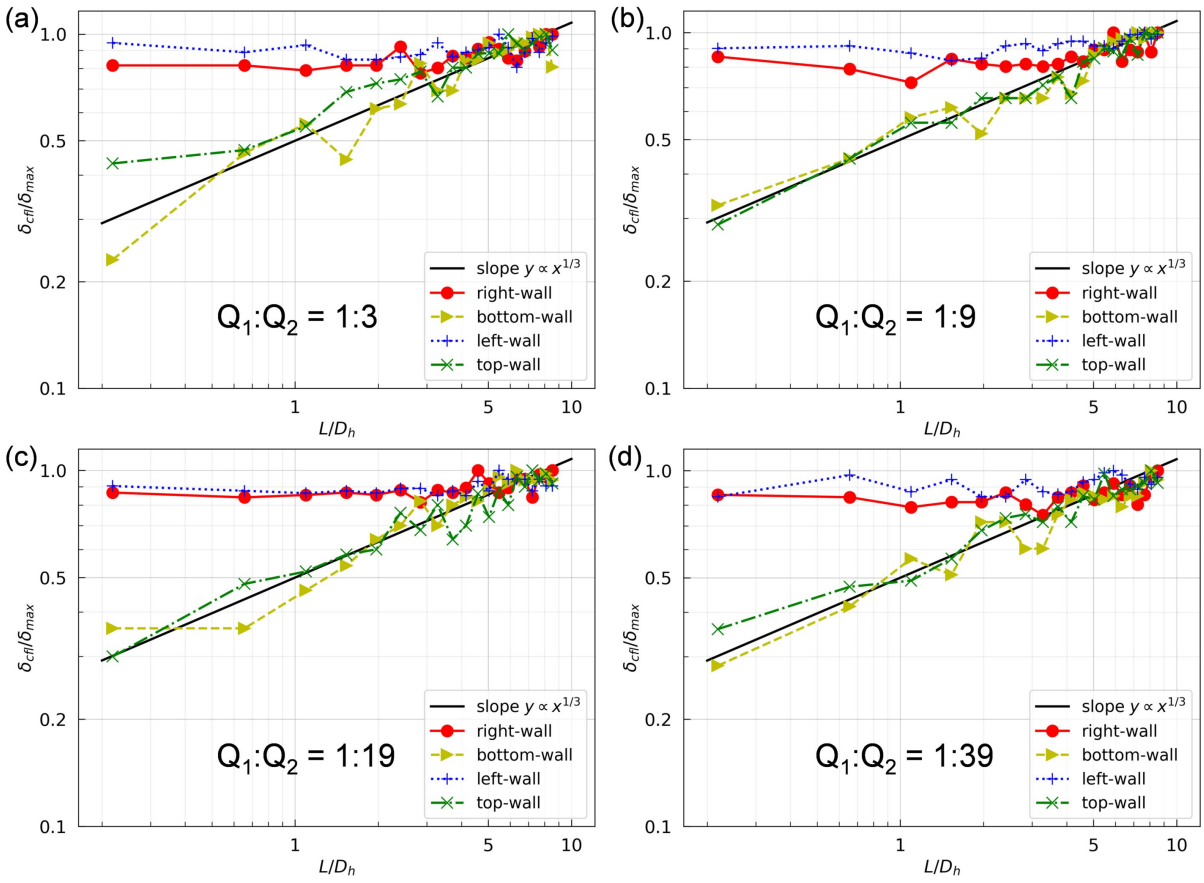

Figure S7: (Simulation) Regression analysis of the simulated CFLs in PB, plotted in log-log scale. The CFL thickness δ_{cfl} is normalised by the maximum CFL value δ_{max} detected within the investigated range ($L \approx 10D_{\mathrm{h}}$). The development length L is normalised by the channel hydraulic diameter D_{h}.

S6 Empirical model of phase separation

Up to date, several models have been proposed to describe the partitioning of RBCs at microvascular bifurcations [2, 3, 4]. Among others, the most widely-applied one is probably the phase-separation model (PSM as mentioned in the introduction) developed by Pries *et al.* based on *in vivo* experiments and theoretical modelling [2, 5]. In brevity, the PSM derived a set of empirical equations from experimental observation of RBCs at arteriolar bifurcations in rat mesentery, and established a flow-mediated mechanism to quantitatively describe the RBC fluxes received by child branches of diverging bifurcations within a microvascular network.

The PSM correlates the fractional RBC flow FQ_E in a child vessel of a divergent bifurcation with the fractional blood flow FQ_B that it receives:

$$FQ_E = \begin{cases} \frac{1}{1+\mathrm{e}^{-[A+B\ln(\frac{FQ_B-X_0}{1-(FQ_B+X_0)})]}}, & X_0 < FQ_B < 1-X_0 \\ 0, & FQ_B \leq X_0 \\ 1, & FQ_B \geq 1-X_0 \end{cases} \tag{S1}$$

where A, B and X_0 are fitting parameters obtained *via* linear regression analysis. A reflects the size difference of the two child vessels, B reflects the shape of the haematocrit profile in the parent vessel and X_0 is related to the corresponding thickness of cell-depleted layer (or cell-free layer). According to [2, 6]:

$$A = -13.29[(D_\alpha^2/D_\beta^2 - 1)/(D_\alpha^2/D_\beta^2 + 1)](1 - H_D)/D_F \tag{S2}$$

$$B = 1 + 6.98(1 - H_D)/D_F \tag{S3}$$

$$X_0 = 0.964(1 - H_D)/D_F \tag{S4}$$

wherein D_α, D_β and D_F are diameters (formulated in μm) of the two child branches and the parent branch, respectively. H_D is the discharge haematocrit in the parent branch.

Table S2: (Simulation) Relative errors of the simulated RBC fluxes at the primary Y-type bifurcation against predictions made by the empirical model [5], see Figure 4e.

Child branch	$Q_2/Q_1 = 1$	$Q_2/Q_1 = 3$	$Q_2/Q_1 = 9$	$Q_2/Q_1 = 19$	$Q_2/Q_1 = 39$
High flow	0.4%	0.8%	0.2%	0.1%	0.2%
Low flow	0.8%	1.0%	0.3%	0.4%	0.2%

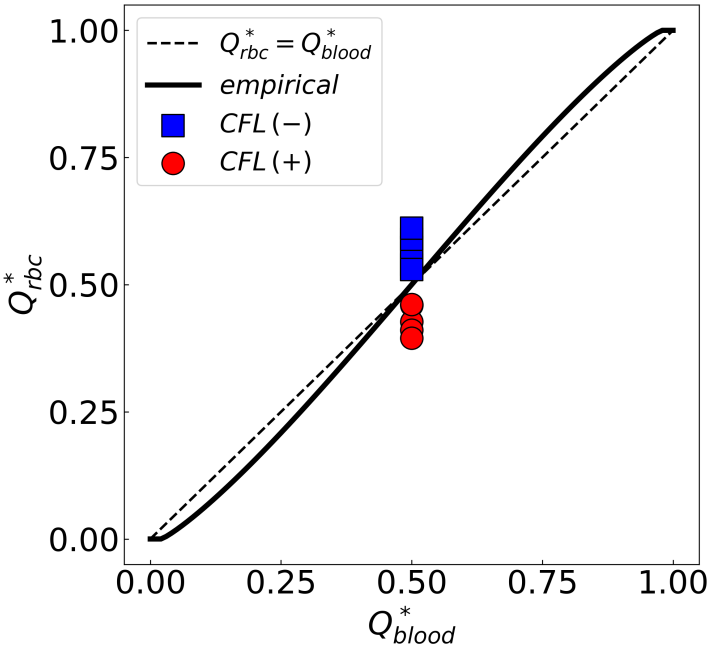

Figure S8: (Simulation) Comparison of the simulated distribution of RBC fluxes at BifT2 against the empirical model [5], following the same convention as Figure 4e.

S7 Haematocrit reduction/enrichment in network

Table S3: (Simulation) Discharge haematocrits H_D measured in the network (for the feeding branch PB it is referred to as $H_{D,\text{inflow}}$). The designed feeding haematocrit at the flow inlet is $H_F = 1\%$, unless otherwise stated. If any child branch has its H_D larger than that of the feeding branch, *i.e.* $H_{D,\text{inflow}}$, that child branch experiences haematocrit enrichment (marked by $\star$); otherwise, the branch experiences haematocrit reduction or the haematocrit keeps unchanged).

Q_2/Q_1	PB	CB11	CB12	CB21	CB22	CB23	CB24
1	1.02%	1.04% ($\star$)	1.02%	0.80%	1.27% ($\star$)	1.24% ($\star$)	0.80%
3	1.03%	0.81%	1.09% ($\star$)	0.63%	1.00%	1.16% ($\star$)	1.01%
9	0.99%	0.61%	1.03% ($\star$)	0.33%	0.87%	1.22% ($\star$)	0.85%
19	0.99%	0.28%	1.03% ($\star$)	0	0.42%	1.18% ($\star$)	0.88%
39	0.99%	0	1.01% ($\star$)	0	0	1.09% ($\star$)	0.93%
9 ($H_F = 2\%$)	2.03%	1.21%	2.12% ($\star$)	0.67%	1.79%	2.49% ($\star$)	1.77%
9 ($H_F = 10\%$)	10.05%	6.76%	10.40% ($\star$)	4.48%	8.84%	11.28% ($\star$)	9.60%

References

[1] Qi Zhou, Joana Fidalgo, Lavinia Calvi, Miguel O. Bernabeu, Peter R. Hoskins, Mónica S. N. Oliveira, and Timm Krüger. Spatiotemporal Dynamics of Dilute Red Blood Cell Suspensions in Low-Inertia Microchannel Flow. *Biophysical Journal*, 118(10):2561–2573, 2020.

[2] A. R. Pries, K. Ley, M. Claassen, and P. Gaehtgens. Red cell distribution at microvascular bifurcations. *Microvascular Research*, 38(1):81–101, 1989.

[3] Ian G. Gould and Andreas A. Linninger. Hematocrit Distribution and Tissue Oxygenation in Large Microcirculatory Networks. *Microcirculation*, 22(1):1–18, 2015.

[4] Jiho Yang, Sung Sic Yoo, and Tae-Rin Lee. Effect of fractional blood flow on plasma skimming in the microvasculature. *Physical Review E*, 95(4):040401, 2017.

[5] A. R. Pries, B. Reglin, and T. W. Secomb. Structural response of microcirculatory networks to changes in demand: information transfer by shear stress. *American Journal of Physiology - Heart and Circulatory Physiology*, 284(6):H2204–H2212, 2003.

[6] A. R. Pries and T. W. Secomb. Microvascular blood viscosity in vivo and the endothelial surface layer. *American Journal of Physiology - Heart and Circulatory Physiology*, 289(6):H2657–H2664, 2005.